THE EFFECT OF TEMPERATURE ON THE MICROSTRUCTURES OF ADDITIVELY MANUFACTURED TI6AL4V(ELI)

T.D. MOLOI [1,*], T.C. DZOGBEWU [1], M. MARINGA [1], AND A.M. MUIRURI [2]

[1] Department of Mechanical and Mechatronics Engineering, Central University of Technology, Free State, Private Bag X20539, Bloemfontein 9300, South Africa. Website: www.cut.ac.za; Email: *moloitd7@gmail.com**, *dzogbewu@cut.ac.za*, *mmaringa@cut.ac.za*

[2] Department of Mechanical Engineering, Muranga University of Technology, P.O. Box 75-10200, Muranga, Kenya. Website: www.mut.ac.ke; E-mail: *amuiruri@mut.ac.ke*

Abstract: The stability of microstructure at high temperatures is necessary for many applications. This paper presents investigations on the effect of changes in temperature on the microstructures of additively manufactured Ti6Al4V(ELI) alloy, as a prelude to high temperature fatigue testing of the material. In the present study, a Direct Metal Laser Sintering (DMLS) EOSINT M290 was used to additively manufacture test samples. Produced samples were stress relieved and half of these were then annealed at high temperatures. The samples were then heated from room temperature to various temperatures, held there for three hours and thereafter, cooled slowly in the air to room temperature. During tensile testing, the specimens was heated up to the intended test temperature and held there for 30 minutes, and then tensile loads applied to the specimens till fracture. Metallographic samples were then prepared for examination of their microstructures both at the fracture surfaces and away from them. The obtained results showed that changes in temperature do have effects on the microstructure and mechanical properties of Ti6Al4V(ELI) alloy. It is concluded in the paper that changes in temperature will affect the fatigue properties of the alloy.

Keywords: Effect of temperature, Microstructure, Mechanical properties, Additive manufacturing, Ti6Al4V(ELI), Heat treatment.

1. INTRODUCTION

Additive Manufacturing (AM) was established in 1987, as a solution for faster product development. Additive Manufacturing is the process of joining materials to make objects from 3D model data, usually layer upon layer, as opposed to subtractive manufacturing methodologies such as casting, moulding, forming, machining, or joining [1]. For metallic materials, AM is common to use powder feedstocks that are melted successively using a directed energy source such as a laser or electron beam [2]. Subtractive manufacturing methodologies of Ti6Al4V parts often forge or cast material before machining parts to final shapes and dimensions, which unavoidably results in a large amount of material waste and long lead times [3]. Additive manufacturing technologies are used to manufacture Ti6Al4V parts at high build temperatures in the ranges of 1660 to 1670 *°C* [3, 4]. Such high build temperatures with their rapid cooling rates result in parts with different microstructures and material properties, as compared to conventional manufacturing methodologies [3]. Laser-powder-bed-fusion (LPBF) technologies are widely used to produce titanium alloy parts. These technologies include selective laser melting (SLM), selective laser sintering (SLS), laser metal fusion (LMF), and direct metal laser sintering (DMLS) [5-6]. The DMLS is an additive manufacturing technology that can be used to prototype one-off parts or manufacture low-volume production that runs directly from Computer Aided Drawing (CAD) data [2]. The DMLS technology has the ability to produce fine features and thin walls with good accuracy; works well with a wide variety of elemental metals and alloys and provides excellent resolution of features [2].

During the building process, the printed layers go through repeated melting and solidification. When the printed layers restrain the contraction of the current layer, this results in the creation of residual stresses in fabricated parts. Residual stresses can cause initiation cracks and ultimately reduce the fatigue lives of parts [7]. The post heat treatment process of stress relieving is applied to remove residual stresses present in the DMLS as-built parts [8]. The rapid cooling inherent in DMLS results in the formation of a needle-like microstructure called acicular *α*' martensitic microstructure. This microstructure is formed as a result of cooling at rates in the range of 10^4 - 10^6 *K/s*, of the alloy from the high temperatures in the *β*-field during the DMLS process [9]. The acicular α' martensitic microstructure is undesirable due to its characteristics of brittleness. High temperature annealing heat treatment is applied to transform this unstable needle-like microstructure to stable mixture of *α*- and *β*-phases. When the temperature is high enough, the thermal energy of atoms increases and causes the atoms to migrate and overcome the surface energy of the grain boundaries. This results in the movement of grain boundaries and the growth of

[DOI: 10.22068/ijmse.3589]

grains. Therefore, higher temperatures imposed on Ti6Al4V(ELI) lead to higher mobility of grains and the attendant coarsening of α-laths [10-11].

Several industries such as aerospace, biomedical, and automobile, use titanium alloys for many applications at room and high temperatures. Stability at high temperatures is necessary for many applications [12-14]. The Ti6Al4V alloy is the most widely studied titanium alloy and is often regarded as the workhorse of the alloys of titanium. It is a dual-phase (α+β)- titanium alloy with high strength, low density, high fracture toughness, excellent corrosion resistance and superior biocompatibility [3]. The Ti6Al4V alloy is commonly used at normal room temperature and up to temperatures of 250-400 $°C$ [15]. Zhao *et al*. [15], reported that the application of the alloy at temperatures above 400 $°C$ can affect its microstructures. To the contrary, Song *et al*. [16], reported that the microstructure of SLM-built samples has little sensitivity to a temperature below 500 $°C$ and that only above 500 $°C$ did changes occur. The difference between the two studies is the soaking time, Zhao *et al*. [15], soaked samples for four hours while Song *et al*. [16], soaked samples for half an hour. Zöllner [10], demonstrated that variation of temperature has a significant effect on the growth of grains.

The Ti6Al4V alloy occurs in the form of various microstructures, namely lamellae, equiaxed, martensitic, bimodal and Widmanstätten. Lamellae microstructure has good creep and high fatigue crack growth resistance, while equiaxed has high fatigue crack initiation resistance. The bimodal microstructure combines both the advantages of lamellar and equiaxed microstructures and possesses an excellent combination of strength and ductility [17-18]. High cooling rates of the alloy that are greater than 410 $°C/s$ results in the formation of a complete martensitic microstructure [3]. This microstructure is characterized by high strength and hardness. The bimodal and equiaxed microstructures are formed during recrystallization. Lamellae microstructure is formed as a result of the transformation of β-grains to α+β grains during slow cooling from the high temperature single-phase β region [17, 19]. The alloy's mechanical properties such as yield strength, ultimate tensile strength, and percentage elongation are dependent on the microstructure of the alloy [3, 20]. The microstructure of the alloy in turn is dependent on the properties of the powder used, process parameters and part geometry [21].

The mechanical properties of metallics define their response to applied loads. Key amongst these mechanical properties are strength, ductility, modulus of elasticity, and hardness [22]. Microstructural features such as grain morphologies and sizes as well as texture do determine the mechanical properties of metallics [23-24]. The mechanical properties of Ti6Al4V have been noted to be sensitive at all temperatures [16]. At high temperatures strength, hardness, and modulus of elasticity of the alloy decrease while ductility increases, whereas at low temperatures strength, hardness, and modulus of elasticity increase, while ductility decreases [16].

Many studies have focused on the effect of heat treatments on the microstructure and tensile properties and less work has been done on the effect of temperature. This study aims to investigate the effect of temperature on the microstructure and mechanical properties of the alloy. The novelty arising from this research lies in the emergence of a definitive statement based on systematic testing, of the dependence on test temperatures lying between 20 $°C$ and 350 $°C$, of the microstructure of as-built, stress relieved, as well as stress relieved then high temperature annealed specimens of Ti6Al4V(ELI) specimens, for use in elevated temperature fatigue testing.

2. EXPERIMENTAL PROCEDURES

2.1. Preparation of Samples

In this study, a DMLS EOSINT M290 machine was used to manufacture all test samples. The machine was set to the optimum process parameters shown in Table 1, as recommended by the manufacturing company EOS GMBH for the production of Ti6Al4V parts.

Table 1. Process Parameters for Ti6Al4V(ELI) Manufactured By DMLS EOSINT M290

Parameters	Laser power (W)	Hatch spacing (μm)	Layer thickness (μm)	Scanning speed (mm/s)	Laser diameter (μm)
Ti6Al4V(ELI)	280	120	40	1300	80-100

Two sets of samples were manufactured. The first set of samples for soaking at different temperatures and were built as cube blocks with the dimensions of 10 mm. The tensile test samples were

[DOI: 10.22068/ijmse.3589]

manufactured as rods of 53 *mm* in length and 12 *mm* in diameter and then further machined to comply with ASTM E8 standards. Eighteen samples per set were manufactured.

2.2. Post Heat Treatment Processes

Two samples were tested without any heat treatment and are referred to as, as-built samples. The two sets of samples were stress relieved and half of those were further annealed at a high temperature. Stress relieve heat treatment was done while the samples were still attached to the building substrate. In this process, the samples were heated to 600 °*C* at the rate of 0.08 °*C/s*, held at this temperature for 3 hours and then furnace-cooled in a vacuum to room temperature. This stress relieving heat treatment regime was adopted from the works carried out over the past years, that showed it to effectively relieve residual stress without affecting the microstructure of the as-built part. Half of the stress relieved samples were then cut off from the building substrate for inspection. The remaining samples were exposed to high temperature annealing while still attached to the building substrate. In this process, the samples were heated temperature at the rate of 0.13 °*C/s* to the beta transus temperature of 980 °*C* and held at this temperature for 1 hour; then furnace cooled to 705 °*C*, held at this temperature for 2 hours; and then vacuum cooled back to room temperature. The temperature of 980 °*C* was selected ensure transformation of the microstructure from the α- to β-grains and soaking carried out at this temperature to ensure homogenisation of the resulting microstructure. Furnace cooling at a temperature of 705 °*C* was carried out to ensure the transformation of β-grains to α-grains and their growth in size to enhance ductility of the alloy.

2.3. Soaking of Samples at Various Elevated Temperatures

The samples that were heat treated were further soaked at these temperatures 133 °*C*, 241 °*C* and 349 °*C*. These soaking temperatures were selected to fall below the maximum normal operating temperature of 400 °*C* noted in the literature, below which it has been observed in literature that temperature has no effect on the microstructure, and therefore, served to test this inference. Two stress relieved and two high temperature annealed samples were soaked at each temperature for three hours and then cooled slowly in the air to room temperature. Table 2 presents the DMLS Ti6Al4V(ELI) sample groups.

Table 2. DMLS Ti6Al4V(ELI) sample groups

Sample Group	Status/Heat Treatment
A	As-built
B	Stress relieved
C	Stress relieved and then high temperature annealed
D	Sample B soaked at 133 °*C*
E	Sample C soaked at 133 °*C*
F	Sample B soaked at 241 °*C*
G	Sample C soaked at 241 °*C*
H	Sample B soaked at 349 °*C*
I	Sample C soaked at 349 °*C*

2.4. Metallographic Examination

Metallographic examination was done on all the built specimens. To do this, the specimens that were cut from them were mounted in a mounting cylinder in Multifast resin using a Struers Mounting Press Citopress machine. Two samples that had undergone similar heat treatment processes were taken for metallographic analysis. For the soaked samples, the top surface (perpendicular to the build direction) of one sample and side surface (parallel to the build direction) of the other sample were left free during mounting for analysis; while for the tensile test samples, the surfaces that were cut along the longitudinal z-build direction were left free for analysis. The cut surfaces were ground using a 320-grit size silicon carbide (SiC) grinding paper with water as a lubricant using a Struers tegramin machine. This was followed by polishing at three stages to obtain a mirror finish surface. Polishing was carried out on Struers tegramin machine, using a Largo Diapro cloth, with a 9 μm diamond suspension for 5 minutes, then using a Mol Diapro cloth for 2 minutes, and then the final stage of polishing was done using an MD-Chem cloth with a 4 μm suspension of diamonds for 110 seconds. Kroll's reagent (Water 92.82 %, Nitric Acid 6.11 %, and Hydrofluoric Acid 1.07%) was used to etch the samples to reveal their

[DOI: 10.22068/ijmse.3589]

microstructures. Thereafter, a Zeiss Axio A1 optical microscope was used on the etched samples to examine their microstructures.

2.5. Tensile Testing

Tensile testing was conducted on a Servo Instron 1342, H7051 hydraulics testing machine. Two sets of specimens were tested at the three different temperatures of 20 *°C*, 175 *°C*, and 325 *°C*. Three specimens were tested at each temperature. During testing, each specimen was mounted on the testing machine, heated up to the intended test temperature, and kept at this temperature for 30 minutes, following which a tensile load was applied on the specimen at a displacement rate of 2 *mm/min* until failure and complete separation. The tensile properties investigated here were yield strength, ultimate tensile strength, percentage elongation, and modulus of elasticity.

2.6. Vickers Microhardness Testing

After tensile testing, small samples were cut from the uniaxial tensile fractured specimens, and an electrical discharge machine (EDM) wire cutter was used to cut the specimens, along the longitudinal z-build direction. The specimens were then cut in a transverse direction 15 mm away from the fracture surface. Indentations were made on the polished and etched surfaces of the Ti6Al4V(ELI) samples using the Vickers Future Tech FM 7E microhardness tester. Ten indentations were made on each sample under the same conditions, with a test load of 2942 *mN* and a dwell time of ten seconds.

3. RESULTS AND DISCUSSION

3.1. Metallographic Examination of Soaked Samples

3.1.1. The Microstructures of Sample Group A

Fig. 1 shows the top and side view optical micrographs of an as-built Ti6Al4V(ELI) sample produced by DMLS, respectively. It should be noted that the side view and top view are parallel and orthonormal to the build direction, respectively.

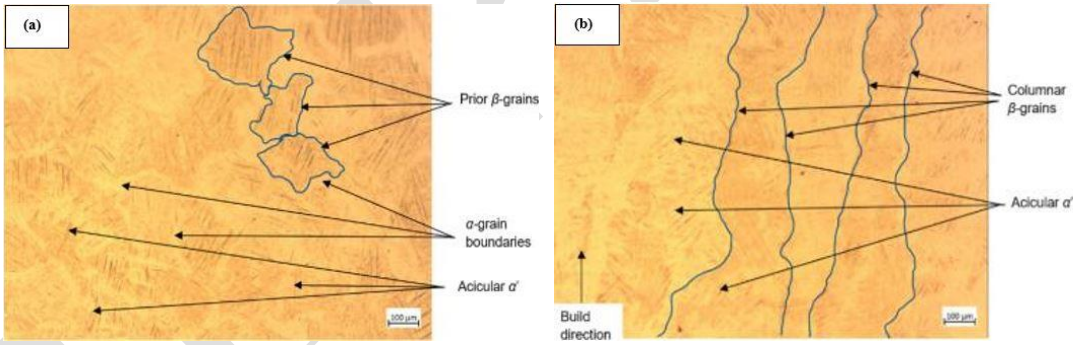

Fig. 1. Optical micrograph of the (a) top and (b) side view of an as-built DMLS Ti6Al4V(ELI) sample

The micrographs in the two figures show different morphologies of prior *β*-grains. Fig. 1(a), which is the top view of an as-built sample, shows a lighter shade needle-like *α*'-lath referred to as *α′* martensite microstructure. The figure also shows epitaxial (columnar) prior *β*-grains whose outlines are shown by blue colour lines on the micrograph and which are separated by *α*-grain boundaries. Fig. 1(b) shows the side view of the sample, consisting of columnar *β*-grains whose outlines are shown the continuous blue colour lines superimposed on the micrograph. These grains grow epitaxially perpendicular to the direction of travel of the laser beam and in the direction of the build [25]. This is mainly due to the temperature gradient of the molten pool being essentially perpendicular to the scanning direction during the DMLS process. The average width of the columnar *β*-grains was measured to be 136±16 *μm* with a coefficient of variance of 11.8 %. Such a high value of the coefficient of variance (COV) implies that the data was spread out away from the mean value. Inside these columnar *β*-grains were found *α′* martensitic laths with an average width of about 2.4±0.4 *μm*, and a COV of 16.7 %. This high COV implies a large scatter of the data. The acicular α' martensitic microstructure is formed as a result of rapid cooling (at rates in the range 10^4-10^6 *K/s*) of the alloy from the high temperature in the β-field during the DMLS process [9]. Madikizela *et al*. [26], found *α′*-laths with a width of 0.3-2.4 *μm* for SLM as-built Ti6Al4V samples, while Agius *et al*. [27], reported that the width of the *α′*-laths varies from 1 to 3 *μm*. Phutela *et al*. [28], found an average columnar *β*-grains width of 90 *μm* in SLM as-built Ti6Al4V

[DOI: 10.22068/ijmse.3589]

samples, while Li *et al*. [29], found an average grain diameter of prior β-grains of 135.5 μm on as-fabricated Ti6Al4V samples. The differences between these values are likely to be a result of different process parameters used during the additive manufacturing process of respective specimens.

3.1.2. The Microstructure of Sample Group B

Fig. 2 shows the top and side view optical micrographs of stress-relieved Ti6Al4V(ELI) samples, respectively.

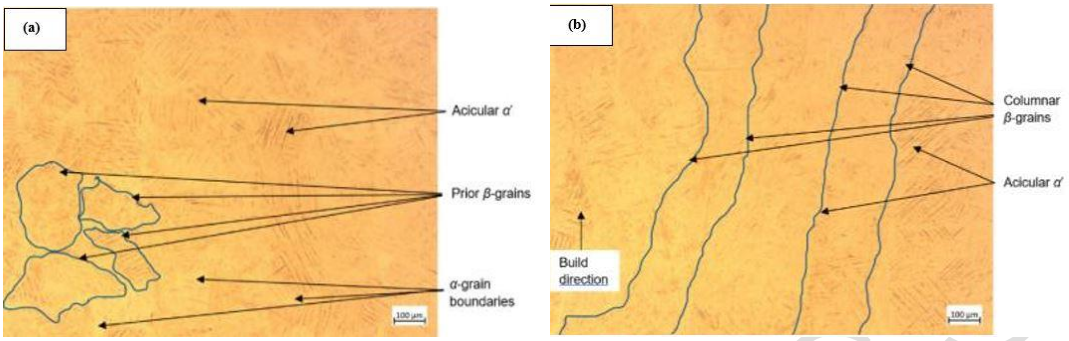

Fig. 2. Optical micrograph of the (a) top view (perpendicular to the build direction) and (b) side view (parallel to the build direction) of a stress-relieved DMLS Ti6Al4V(ELI) sample

The microstructures in Fig. 2(a) and Fig. 2(b) show similar morphologies as those of the as-built samples presented in Fig. 1(a) and Fig. 1(b), respectively. In Fig. 2(a), the acicular α' laths are still visible, with an average width of about 2.6±0.47 μm. The COV for these statistical measures is 18.1 %, which implies a large scatter of data. The mean and standard deviations are 0.2 and 0.07 μm higher, respectively, than the ones for as-built samples shown in Fig. 2(a), a respective increase of 8 and 17 %. Fig. 2(b) shows columnar β-grains which were also evident in the side view of as-built samples. Within these columnar β-grains exist acicular α' laths suggesting that no noticeable microstructure transformation took place during stress-relieving heat treatment as observed under an optical microscope. The average width of the columnar β-grains in Fig. 2(b) was measured to be 142±17 μm, giving rise to a COV of 11.9 %. Jazdzewska *et al*. [30], reported that stress relieving does not affect the mechanical properties of titanium alloys such as strength or ductility but rather only reduces residual stresses. This is consistent with the observation made here that there was no variation of microstructure with stress relieving heat treatment.

3.1.3. The Microstructure of Sample Group C

Fig. 3 shows the top and side view optical micrographs of stress relieved and then high temperature annealed Ti6Al4V(ELI) samples, respectively.

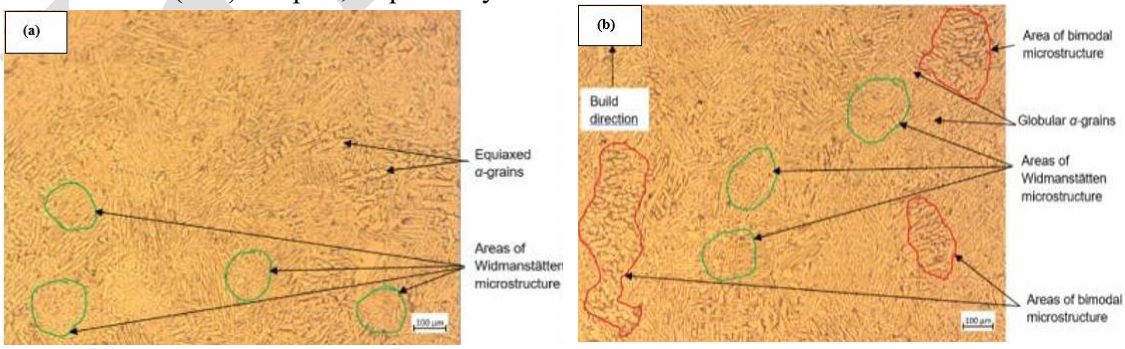

Fig. 3. Optical micrograph of the (a) top view (perpendicular to the build direction) and (b) side view (parallel to the build direction) of a sample stress relieved and then at high temperature annealed DMLS Ti6Al4V(ELI) sample

The morphologies of the microstructure in Fig. 3 are completely different from the ones in Fig. 1 and Fig. 2. This difference in microstructure is due to the differences in the heat treatment processes. In Fig. 3(a), acicular α' needles-like structures no longer exist and are replaced by larger globular α-laths that are longer and wider. When the temperature is high enough, the thermal energy of atoms increases and causes the atoms to migrate and overcome the surface energy of the grain boundaries. This results in the movement of grain boundaries and the growth of grains. Therefore, higher temperatures imposed

[DOI: 10.22068/ijmse.3589]

on Ti6Al4V(ELI) lead to higher mobility of grains and the attendant coarsening of α-laths [10-11]. Fig. 3(a) exhibits a mixture of equiaxed and lamellar α-laths. Both the micrographs in Fig. 3 consist of globular α-laths and Widmanstätten microstructure, the latter shown inside green colour circles boundaries on the micrographs. Fig. 3(b) shows part of the micrographs to exhibit bimodal microstructures some of which are shown inside red coloured contours lines. The average width of the α-laths is about 8.2±1.2 µm, and therefore, a COV of 14.6 %. The average width of the β-laths is about 1.2±0.25 μm, which gives a COV 20.8 %. Such a COV implies a large scatter of the data. Malefane *et al*. [31], in their study of the microstructures on DMLS Ti6Al4V high-temperature annealed samples, observed equiaxed and basket weave microstructures. It was further reported in their research that the average width of the α-laths built in the y-direction was 6.7 μm. The different result between the present study and that of Malefane *et al*. [31], is likely due to differences in the annealing processes used. In their study the annealing was done at a temperature of 950 °*C*, soaking for two hours and cooling at 0.13 °*C/s* to room temperature. In the present study annealing was done at 980 °*C*, soaking was done for one hour, followed by very rapid cooling to a temperature of 705 °*C*, and then soaked for 2 hours followed by cooling at 0.03 °*C/s* to room temperature. The higher initial soaking temperature and slower eventual cooling rate are likely causes of the coarser α-laths obtained in the present study. Zöllner [10], stated that higher temperatures lead to even coarser α-laths. Jovanovic´ *et al*. [32], reported that the thickness of the α-laths increases as the annealing temperature is increasing. They found that the average thickness of the α-laths at temperatures of 1100 °*C*, 950 °*C* and 800 °*C* were 9 μm, 7 μm and 6 μm, respectively.

3.1.4. The microstructure of Sample Group D

Fig. 4 shows the top and side view optical micrograph of stress relieved Ti6Al4V(ELI) samples, respectively, that were soaked at a temperature of 133 °*C* for three hours and allowed to cool slowly in the air.

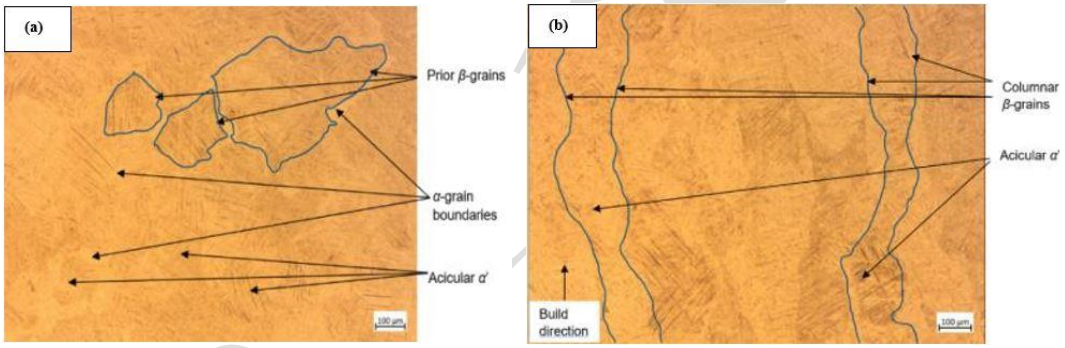

Fig. 4. Optical micrograph of the (a) top view (perpendicular to the build direction) and (b) side view (parallel to the build direction) of a DMLS Ti6Al4V(ELI) sample stress relieved and then soaked at 133 °*C* for three hours

The morphology of the microstructure in Fig. 4(a) is similar to the one in Fig. 2(a). Fig. 4(a) consists of needle-like α' martensite laths, with an average width of about 2.64±0.55 μm and therefore, a COV of 20.8 %. This high COV implies a wide dispersal of data. The mean standard deviations are 0.24 and 0.15 higher respectively, than the ones for as-built samples shown in Fig. 2(a), a respective increase of 10 and 38 %. This implies a modest increase of the size of laths and a significant increase in the scatter of data of size between this case and the one for Fig. 2(a). Fig. 4(a) exhibits prior β-grains whose outlines are shown in blue colour lines and are separated by α-grain boundaries. As was the case in Fig. 2(b), the columnar β-grains in this figure have within them α' martensitic laths. The average width of the columnar β-grains, in this case, is about 144±16 μm. Giving rise to a COV of 11.1 %. This is a further increase above the values of 142±17 μm and 136±16 μm, recorded for the as-built and stress relieved specimens, respectively. Whilst there is a fair increase in the average width of the epitaxial grains from the as-built to stress relieved samples (4 %), the further increase due to soaking at a temperature of 133 °*C* after stress relieving is small (1 %). Clearly, the soaking temperature is too low to have a notable influence on the microstructure as was observed in the study done by Zhao *et al*. [15] and Song *et al*. [16].

3.1.5. The Microstructure of Sample Group E

Fig. 5, shows the top and side views optical micrographs respectively, of DMLS Ti6Al4V(ELI) samples that were stress relieved and then annealed at high temperature and then further soaked at a temperature of 133 °*C* for three hours, followed by slow cooling in air.

[DOI: 10.22068/ijmse.3589]

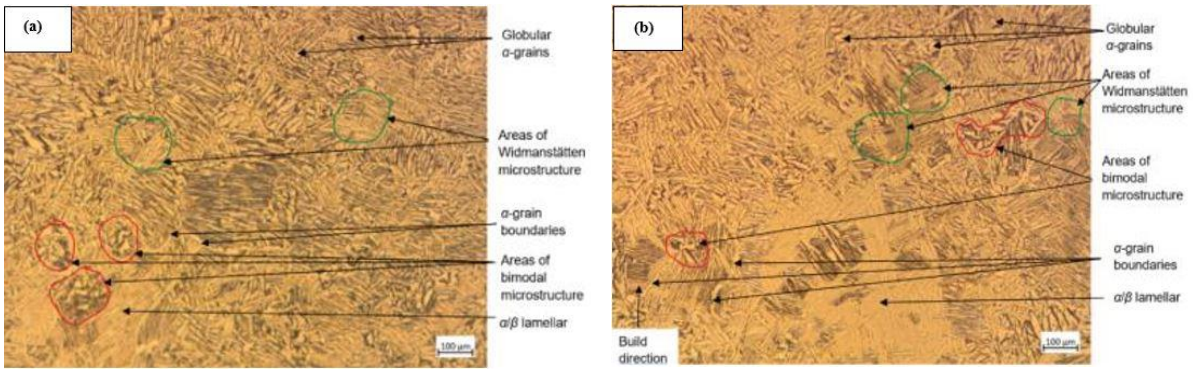

Fig. 5. Optical micrograph of the top view (perpendicular to the build direction) of a stress relieved, high temperature annealed and then soaked at 133 °*C* DMLS Ti6Al4V(ELI) sample

In Fig. 5, the α- and β-phases are clear, with the α-laths being brighter and β-laths darker as shown by the arrows in these figures. In both these two figures, α-grain boundaries, globular α-laths, Widmanstätten and lamellar as well as bimodal microstructures are present. The Widmanstätten and bimodal microstructures are outlined with green and red colour lines on the micrographs, respectively. It can be noted that the micrograph in Fig. 5(b) is dominated by a Widmanstätten microstructure. This microstructure is known to have low strength and poorer ductility among the different microstructures of Ti6Al4V [33]. Fig. 5(a) and Fig. 5(b) show an average width of α-laths of 8.3±1.4 μm, giving rise to a COV of 16.9 %. The average width of α-laths has increased from 8.2 to 8.3 μm when compared with the value recorded from Fig. 3(b) with only stress reliving followed by high temperature annealing. This is a small negligible increase of 1 % that indicates the effect of soaking at a temperature of 133 °*C*, on the width of α-laths is inconsequential. Moreover, the two means fall within the standard deviations of one another. The average width of β-laths was measured at 1.8±0.45 μm, implying a COV of 25 %. This high percentage implies a large spread of data away from the mean value. It is noted that the mean value of width for β-laths has increased from 1.2 to 1.8 μm when compared with the value obtained from Fig. 3(b). This is a much greater (50 %) than was recorded for the α-laths and is a sign that the effect of soaking at 133 °*C* on the growth of β-laths is significant effect of. This increase in the width of β-laths is a sign of a significant increase in the mobility of atoms and is expected to give rise to improved ductility of the alloy [34].

3.1.6. The Microstructure of Sample Group F

Fig. 6, shows the top and side view optical micrographs of stress relieved DMLS Ti6Al4V(ELI) samples, respectively that were then soaked at a temperature of 241 °*C* and thereafter cooled slowly in the air.

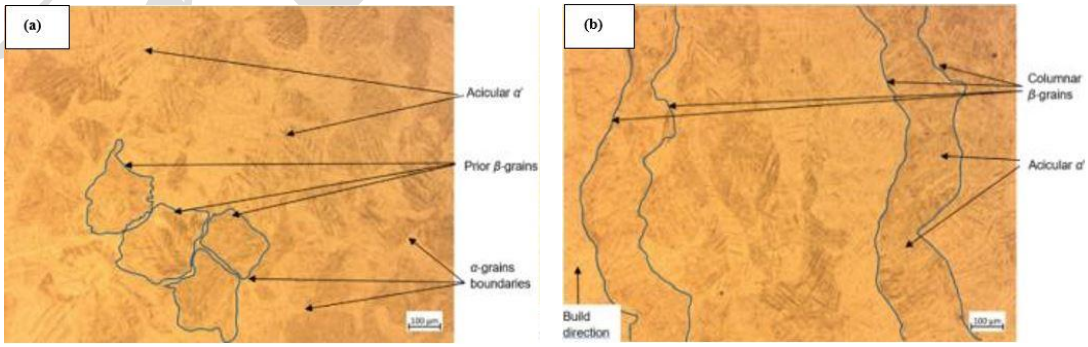

Fig. 6. Optical micrograph of the (a) top view (perpendicular to the build direction) and (b) side view (parallel to the build direction) of a DMLS Ti6Al4V(ELI) stress relieved sample, soaked at a temperature of 241 °*C*

Prior β-grains are evident on the micrograph in Fig. 6(a), whose outlines are shown by blue colour lines and are separated by α-grain boundaries on the micrograph. The acicular α' martensitic microstructure, with an average width of the α' laths of 2.9±0.6 µm exists within these grains, which gives a COV of 20.7 %. This high percentage implies a high dispersion away from the mean value. It is noted that average width of the α' laths has increased from 2.64 to 2.9 μm when compared with the value obtained from Fig. 4(a). This is a small increase of about 1 %, that falls within the standard deviations of both values of mean and therefore, is negligible. Fig. 6(b) shows columnar β-grains whose outlines

[DOI: 10.22068/ijmse.3589]

are shown by continuous blue lines within which exist α' martensite grains. The average thickness of the columnar prior β-grains is about 147±26 μm, giving rise to COV of 17.7 %. This high percentage indicates that the data was highly spread out. The morphology in the above figure shows a predominance of grains that are a bit darker than the one in Fig. 4(a). This is likely due to the higher soaking temperature, which caused an increase in the content of β-laths. Shaikh *et al*. [18], observed an increase in the content of β-laths as the soaking temperature increased.

3.1.7. The Microstructure of Sample Group G

Fig. 7, shows the top and side view optical micrographs of stress relieved and high temperature annealed Ti6Al4V (ELI) samples, respectively that were further soaked at a temperature of 241 °*C* for three hours and then cooled slowly in the air.

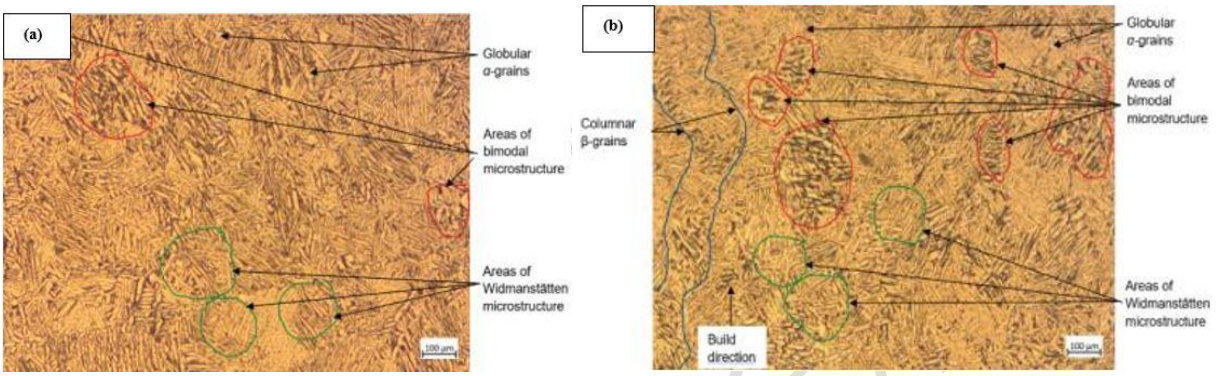

Fig. 7. Optical micrograph of the (a) top view (perpendicular to the build direction) and (b) side view (parallel to the build direction) of a sample soaked at 241 °*C* for three hours, after stress relieving followed by high temperature annealing

Fig. 7 shows the α-laths being brighter and β-laths darker. Both the two figures show globular α-laths, areas of Widmanstätten and bimodal microstructures. The Widmanstätten and bimodal microstructures are circled by green and red colour lines, respectively. A columnar β-grain is visible in Fig. 7(b), whose outline is shown by blue lines, within which are colonies of α- and β-laths. The micrograph in Fig. 7(b) has a high incidence of the bimodal microstructure. This microstructure is known to possess a higher ductility among the microstructures of Ti6Al4V [35-36]. The average width of the α-laths was determined as 8.3±2.3 μm, while the measured average width of the β-laths was 1.9±0.7 μm. The coefficient of variation for the width of the α-laths and β-laths are calculated as 27.7 % and 36.8 %, respectively. Such high percentages suggest a high dispersal of data. It is noted that the width of β-laths had increased by 0.1 μm from the value of 1.8 μm measured in Fig. 5(b), an increase of 6 %.

3.1.8. The Microstructure of Sample Group H

Fig. 8, shows the top and side view optical micrographs of stress relieved Ti6Al4V(ELI) samples, respectively, that were soaked at a temperature of 349 °*C* for three hours and then slowly cooled in the air.

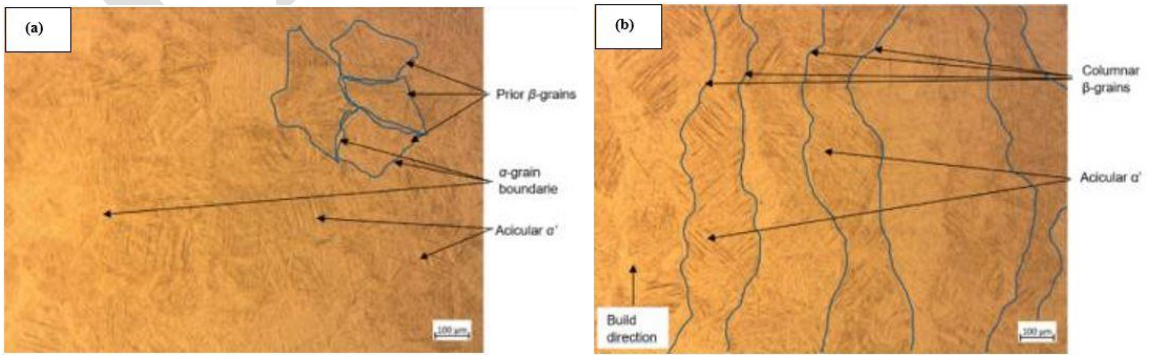

Fig. 8. Optical micrograph of the (a) top view (perpendicular to the build direction) and (b) side view (parallel to the build direction) of a stress relieved DMLS Ti6Al4V(ELI) sample soaked at a temperature of 349 °*C* for three hours

Fig. 8 shows similar morphologies of microstructure as observed in Fig. 6, respectively. Fig. 8(a) shows prior β-grains, with α' martensite laths within them. These prior β-grains are separated by α-grain boundaries. The width of the martensitic α' laths within the prior β-grains in this figure measure to

[DOI: 10.22068/ijmse.3589]

3.1±1.2 μm in width, giving rise to a very high COV of 38.7 %. In Fig. 8(a), it is noted that the width of the α' laths has increased by 0.2 μm from the value of 2.9 μm measured in Fig. 6(a), an increase of 7 %. Agius *et al*. [27], reported that the width of the acicular α' laths vary from 1 to 3 μm for as-built samples. Slightly higher values of the width of the α' martensitic laths were recorded in the present study, which can be ascribed to the higher soaking temperatures in the present work. The columnar prior β-grains in Fig. 8(b) measure of approximately 137±25 μm in the width, giving rise to a COV of 18.2 %. Such a high percentages implies a high dispersal of data.

3.1.9. The Microstructure of Sample Group I

Fig. 9, shows the top and side view optical micrographs of stress relieved and high temperature annealed Ti6Al4V(ELI) samples, respectively that were soaked at a temperature of 349 °C for three hours before being cooled in the air.

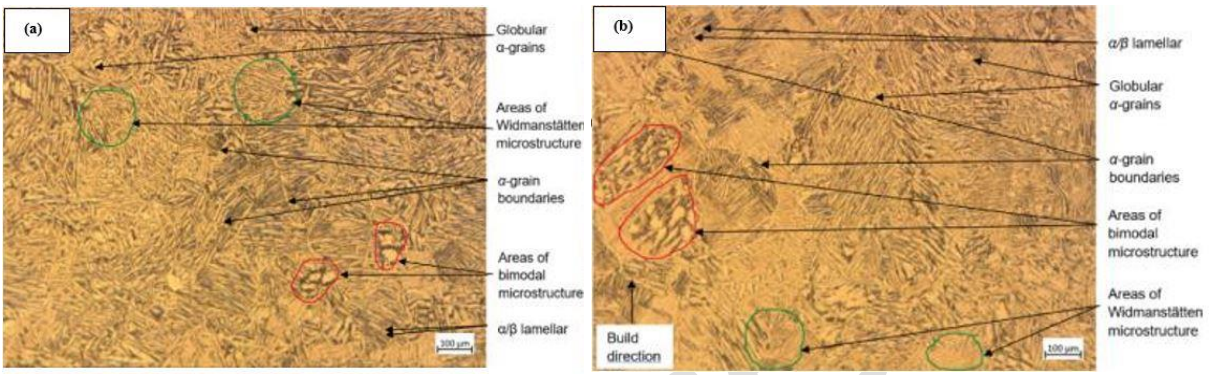

Fig. 9. Optical micrograph of the (a) top view (perpendicular to the build direction) and (b) side view (parallel to the build direction) of DMLS Ti6Al4V(ELI) samples that were stress relieved and then annealed at high temperature followed by soaking at 349 °C for three hours

After being soaked at 349 °C for three hours, the micrographs in Fig. 9 shows a further increase in darker areas compared to Fig. 7. This could be a result of the increase in soaking temperature, which from the transformation phase diagram of the alloy implies higher content of the β-laths. The micrographs show areas of α- and β-phases that are stacked parallel to each other forming a lamellar microstructure. There are also areas of globular α-grains and Widmanstätten microstructure whose outlines are shown by blue colour circles. The two micrographs have areas of bimodal microstructures whose outlines are shown by red colour circles. The bimodal microstructure is known to exhibit a well-balanced strength and ductility [37]. The average width of the α-lath was measured at 8.9±1.9 μm, giving rise to a COV of 21.3 %. The average width of the β-lath measured 2.4±0.3 μm, giving rise to a COV of 12.5 %. Such high percentages suggests that the data was spread out. It is noted that the mean width of the β-lath increased by 0.5 μm from the value of 1.9 µm measured in Fig. 7(a), an increase of 28 %. Shaikh *et al*. [18], observed a similar trend, as the soaking temperature increased. Xing *et al*. [38], stated that as the powder bed temperature increases the width of the β-lath increases as well.

Fig. 10 summarizes the observation made in Fig. 1 to Fig. 9. The symbol SR and HTA denote stress relieved and high temperature annealed, respectively.

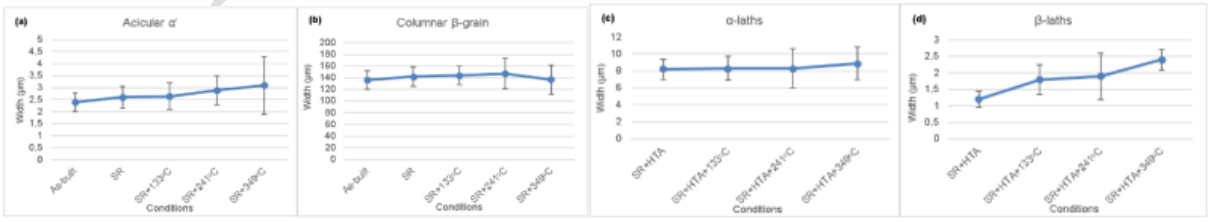

Fig. 10. The average width of the (a) acicular α' laths, (b) columnar β-grains, (c) α-laths and (d) β-laths

Fig. 10(a) shows that as the soaking temperature increases from room temperature to a temperature of 349 °C, the widths of α' laths increase as well. Fig. 10(b) shows that as the soaking temperature increases from room temperature to a temperature of 241 °C, the width of the columnar prior β-grains increases as well. However, at 349 °C the width of the columnar prior β-grains experiences a drop in value. Fig. 10(c) and Fig. 10(d) show that as the soaking temperature increases the width of the α- and

[DOI: 10.22068/ijmse.3589]

β-laths increase. This result is similar to the study done by Zöllner [10], who stated that higher temperatures lead to even coarser α-laths. However, the measured values of mean in all but a few cases in the above figures fall within the error bars, which implies that the differences observed in the graphs are insignificant. It is right to conclude, therefore, that soaking temperatures below 350 *°C* have little to no effect on the microstructure of the Ti6Al4V(ELI) alloy.

3.2. Mechanical Properties

Table 3 shows the obtained results from tensile and hardness testing of stress relieved DMLS Ti6Al4V(ELI) specimens tested at different temperatures.

Table 3. Mechanical Properties of Specimens that were Stress Relieved

Temperature *°C*	Yield Strength (*MPa*)	Ultimate Tensile Strength (*MPa*)	Modulus of Elasticity (*GPa*)	Vickers Micro-Hardness (*HV*)	Percentage Elongation (*%*)
20	1266.7±60.4	1311±52	123.8±5.2	348.6±12.7	5.9±1.6
175	1008.6±85.5	1073.2±66	116.9±0.9	327.3±12.5	7.8±0.4
325	913.8±21.1	993.3±6.2	105.9±3.4	-	10.8±2.9

The data in Table 3 shows that increasing the testing temperature from 20 *°C* to 175 *°C* and 325 *°C* led to a reduction of yield strength, ultimate tensile strength, modulus of elasticity, and hardness, as well as an increase in ductility.

Table 4 shows the obtained results from tensile and hardness testing of stress relieved followed by high temperature annealing DMLS Ti6Al4V(ELI) specimens tested at different temperatures.

Table 4. Mechanical Properties of Specimens that were Stress Relieved Followed by High Temperature Annealing

Temperature *°C*	Yield Strength (*MPa)*	Ultimate Tensile Strength (*MPa*)	Modulus of Elasticity (*GPa*)	Vickers Micro-Hardness (*HV*)	Percentage Elongation (*%*)
20	888.4±33.9	953.7±59	99.5±17	312.5±25.3	13.8±2.1
175	597.2±84.3	674.8±83	91.7±13.5	310.4±33.9	13.9±1.6
325	544.3±33.4	654.9±6.7	83.3±1.1	-	17.3±4.6

Similar to the specimens that were stressed relieved only, increasing the testing temperature led to a reduction of yield strength, ultimate tensile strength, modulus of elasticity, and hardness, as well as an increase of ductility. It is noted that annealing heat treatment led to a reduction of yield strength, ultimate tensile strength, modulus of elasticity, and an increase in ductility.

3.3. Metallographic Examination of Tensile Tested Samples

3.3.1. Microstructures of Samples that were Stress Relieved and then Tested at a Temperature of 20 °C.

Fig.11 show optical micrographs of stress relieved Ti6Al4V(ELI) samples that were tested at a temperature of 20 *°C*

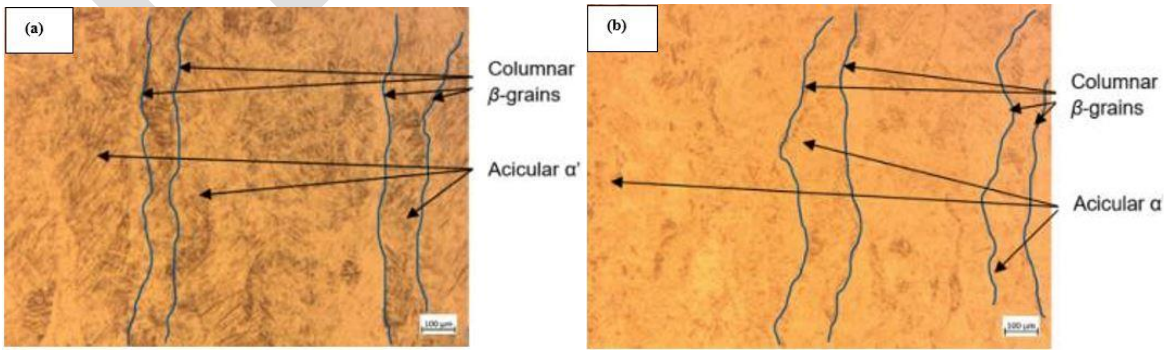

Fig. 11. Optical micrograph of a stress relieved DMLS Ti6Al4V(ELI) sample and tested at a temperature of 20 *°C* (a) near the fracture surface and (b) 15 *mm* away from the fracture surface

The two figures show a needle-like α' lath known (dark lines) martensite microstructure, inside columnar β-grains. The average widths of the columnar β-grains in Fig. 11(a) and Fig. 11(b) are 135±14 μm and 136±11 μm, respectively, with coefficients of variance (COVs) of 10.4 *%* and 8.1 *%*, respectively. The average widths of α' martensitic laths in Fig. 11(a) and Fig. 11(b) are 3.8±0.3 μm and 3.7±0.4 μm, respectively, with COVs of 7.9 *%* and 10.8 *%*, respectively. It is noted that the COVs are

[DOI: 10.22068/ijmse.3589]

high, which implies that the data was spread out away from the mean value. There are small differences in the average values of columnar β-grains and α' martensitic that fall within the respective standard deviations given above for both values of the two means. In Fig. 11(a), the micrograph is darker, and the columnar β-grains are more visible than in Fig. 11(b), this is likely to be a result of lateral (transverse) strains at the neck.

3.3.2. Microstructures of Specimens that were Stress Relieved and Tested at a Temperature of 175 °C.

Fig. 12 shows optical micrographs of stress relieved Ti6Al4V(ELI) samples that were tested at a temperature of 175 *°C*.

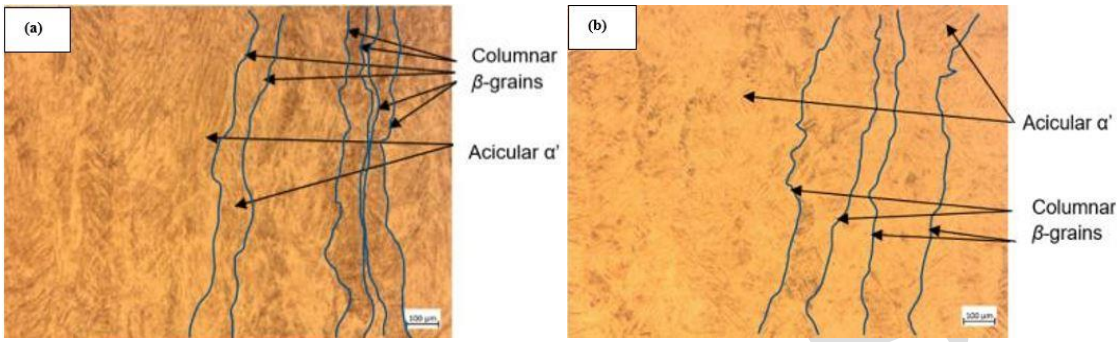

Fig. 12. Optical micrograph of a stress relieved DMLS Ti6Al4V(ELI) sample and tested at a temperature of 175 *°C* (a) near the fracture surface and (b) 15 *mm* away from the fracture surface

The two figures show the presence of columnar β-grains within them α' lath martensitic microstructure. In Fig. 12(a), the average widths of the columnar β-grains and α' laths are 146±13 μm and 3.8±0.4 μm, respectively, with COVs of 8.9 % and 10.5 %, respectively. In Fig. 12(b), the average widths of the columnar β-grains and α' laths are 136±14 μm and 3.7±0.6 μm, respectively, with COVs of 10.3 % and 16.2 %, respectively. Similar to Fig. 11(a) and Fig. 11(b), the calculated values of the COV are high, which reduces the reliability of the calculated values of mean. It is noted that in Fig. 12(a), the columnar β-grains are closely packed and narrower than in Fig. 12(b), which is thought to be a result of the severity of deformation taking place during necking and the attendant transverse, Poisson's ratio contraction.

3.3.3. Comparing Microstructures of Specimens that were Stress Relieved and then Tested at Temperatures of 20 °C and 175 °C.

Both Fig. 11(a) and Fig. 11(a) show micrographs that consist of the columnar β-grains and α' laths. However, in Fig. 11(a) the needle-like structures are smaller, more randomly oriented and dense than in Fig. 12(a). It is reported that these needle-like structures exhibit high strength and hardness [17, 19]. This agrees with the finding from the tensile testing conducted here that, as the test temperature was increased there was a reduction in the values of yield and ultimate strength as well as hardness.

3.3.4. Microstructures of Specimens that were Stress relieved Followed by High Temperature Annealing and then Tested at a Temperature of 20 °C.

Fig. 13 shows optical micrographs of stress relieved followed by high temperature annealing Ti6Al4V(ELI) samples that were tested at a temperature of 20 *°C*.

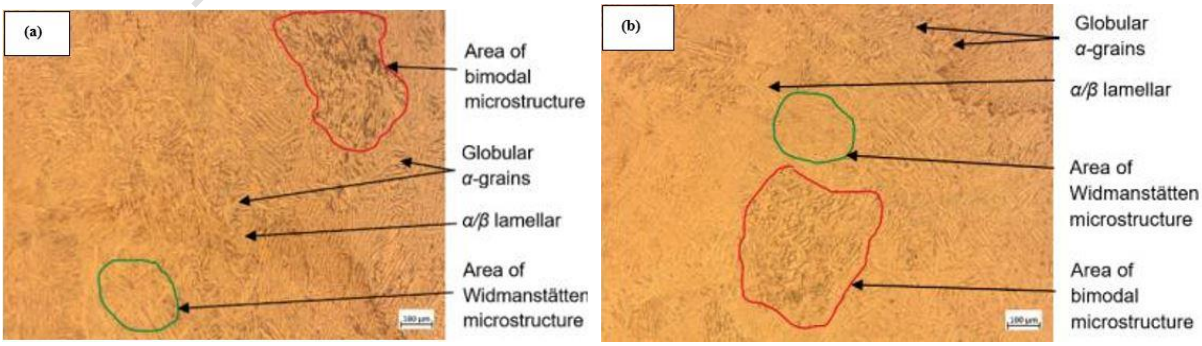

Fig. 13. Optical micrograph of a stress relieved followed by high temperature annealed DMLS Ti6Al4V(ELI) sample and tested at a temperature of 20 *°C* (a) near the fracture surface (b) 15 *mm* away from the fracture surface

[DOI: 10.22068/ijmse.3589]

The two figures show similar micrographs with areas having α- and β-phases that are packed parallel to each other forming lamellar microstructures. There are also areas with Widmanstätten and bimodal microstructures. In Fig. 13(a), the average widths of the α-laths and β-laths were measured at 10.1±0.9 μm and 3.4±0.3 μm, respectively, with COVs of 8.9 % and 8.8 %, respectively. In Fig. 13(b), the average widths of the α-lath and β-lath were measured at 9.1±1.2 μm and 3.4±0.6 μm, respectively, with COVs of 13.2 % and 17.6 %, respectively. It is noted that the average width of α-laths is higher near the fracture surfaces than at 15 *mm* away from the fracture surface, and the average width of β-laths is 3.4 μm in both regions. However, the difference in the first case is small and falls within the standard deviations of the two means.

3.3.5. Microstructures of Specimens that were Stress relieved Followed by High-Temperature Annealing and then Tested at a Temperature of 175 °C.

Fig. 14 shows optical micrographs of stress relieved followed by high temperature annealed Ti6Al4V(ELI) samples and tested at a temperature of 175 °C.

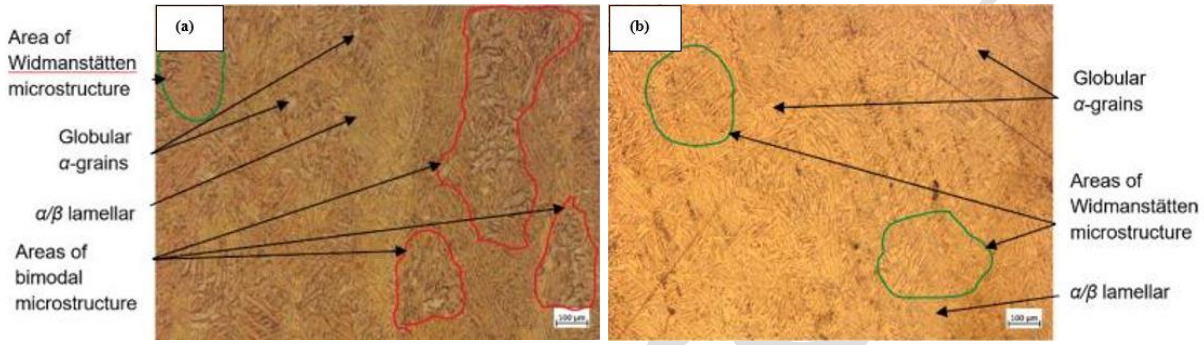

Fig. 14. Optical micrograph of a stress relieved followed by high temperature annealed DMLS Ti6Al4V(ELI) sample and tested at a temperature of 175 °C (a) near the fracture surface (b) 15 *mm* away from the fracture surface

The two figures show both lamellar and Widmanstätten microstructures, with some areas having globular α-grains. Fig. 14(a) shows the presence of bimodal microstructures. In Fig. 14(a), the micrograph is darker than in Fig. 14(b), possibly as a result of transverse strains at the neck. In Fig. 14(a), the average width of the α-lath and β-lath was measured at 13.1±1.2 μm and 4.0±0.4 μm, respectively, with COVs of 9.2 % and 10 %, respectively. In Fig. 14(b), the average widths of the α-laths and β-laths was measured at 9.1±1.0 μm and 3.2±0.4 μm, respectively, with COVs of 11 % and 12.5 %, respectively. These high values of COV, imply data that was scattered away from the mean value. Similar to the samples that were tested at a temperature of 20 °C, the average widths of α-laths and β-laths were greater near the fracture surfaces than at 15 *mm* away from the fracture surface. This is thought to be because of heating effects resulting from the mechanism of necking and fracture.

3.3.6. Comparing Microstructures of Specimens that were Stress Relieved followed by High Temperature Annealing and then Tested at Temperatures of 20 ° and 175 °C.

Both Fig. 13(a) and Fig. 14(a) exhibit globular α-grains, as well as areas of lamellar, Widmanstätten, and bimodal microstructures. The measured average width of the α-lath is greater in Fig. 14(a) than in Fig. 13(a). This is thought to be because of the higher testing temperature. Zöllner [10], reported that increasing temperatures led to coarser α-laths and a reduction in strength. This is consistent with the findings in the present work from tensile and hardness testing, which showed that as the test temperature was raised there was a drop in values of yield and ultimate strength as well as hardness. The average width of the β-laths is wider in Fig. 14(a) than in Fig. 13(a). This is thought to have been due to higher testing temperature, which caused an increase in the width and the content of β-laths as well. This is consistent with the study by Shaikh *et al*. [18]. It has been reported that the β-phase with its body-centered-cubic (BCC) crystal structure is responsible for the ductility of the alloy [15, 32]. The micrograph in Fig. 14(a) has a higher incidence of the bimodal microstructure than the micrographs in Fig. 13(a). The bimodal microstructure is known to possess the highest ductility among the microstructures of Ti6Al4V [35-36]. Again, this agrees with the findings from tensile testing in the present work that as the test temperature was raised the ductility increased.

[DOI: 10.22068/ijmse.3589]

3.4. Comparing the Microstructures of the Soaked Samples to the Microstructures of Tensile Tested Samples Near the Fracture Surface.

Fig. 15 shows optical micrographs of stress relieved Ti6Al4V(ELI) samples.

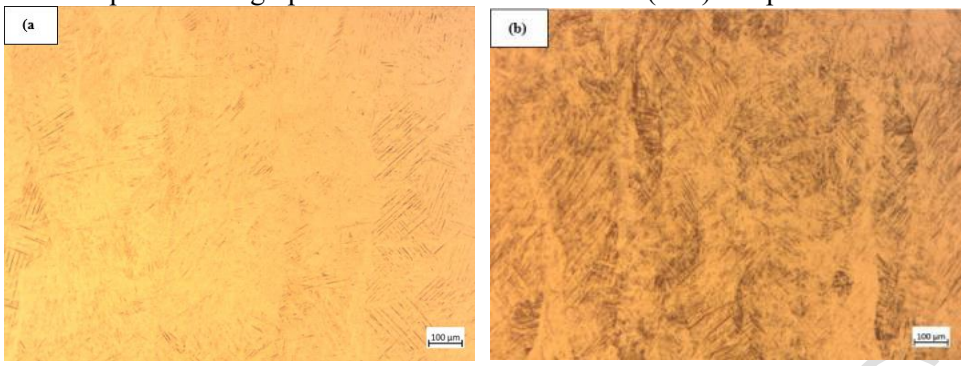

Fig. 15. Optical micrographs of stress relieved DMLS Ti6Al4V(ELI) samples (a) soaked at 20 $°C$ (b) soaked and tested till fracture at a temperature of 20 $°C$

The two micrographs show the presence of an α' martensite microstructure and columnar β-grains. It is noted that Fig. 15(b) is darker than Fig. 15(a), which is thought to be a result of transverse strain at the neck. The average widths of the α' lath were measured to be 2.6±0.47 μm for the micrograph in Fig. 15(a) and 3.8±0.3 μm for the micrograph in Fig. 15(b). The average width of the α' laths for the samples tested at a temperature of 20 $°C$ is wider than that of the samples that were only soaked at the same temperature. This is thought to be due to the heating effects during the necking and fracturing of the specimen.

The samples that were soaked at a temperature of 133 $°C$, as well as soaked at 175 $°C$ and tested in tension showed the presence of the α' martensite microstructure and columnar β-grains. The average widths of the α' laths for the sample that was only soaked at a temperature of 133 $°C$ and the sample that was tested at a temperature of 175 $°C$ were 2.64±0.55 μm and 3.8±0.4 μm, respectively. This is likely due to higher soaking temperature, as the sample in Fig. 15(b) was tested at a temperature of 175 $°C$ after being soaked for 30 minutes at that temperature, while the sample in Fig. 15(a) was only soaked at a temperature of 133 $°C$. Both the sample's average widths of the α' laths were observed to increase with the increase in testing and in soaking temperature. The average width of the columnar β-grains varies along the length for both the soaked samples and the tensile tested samples.

Fig. 16 shows optical micrographs of Ti6Al4V(ELI) samples that were stress relieved followed by high temperature annealing.

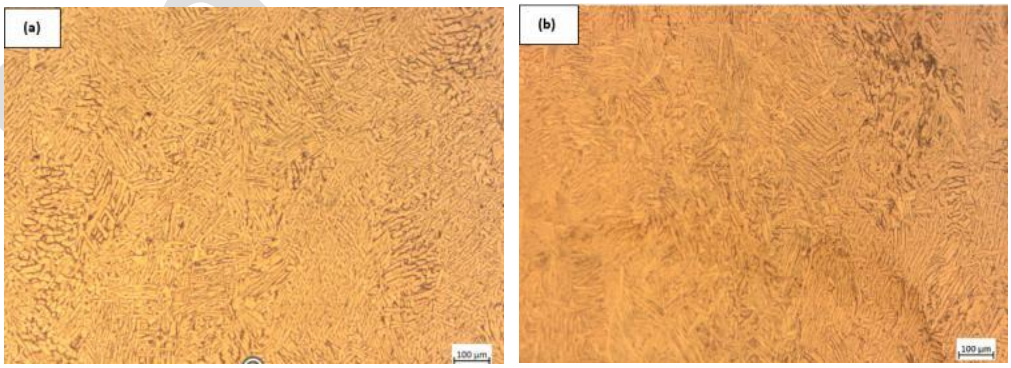

Fig. 16. Optical micrographs of stress relieved followed by high temperature annealed DMLS Ti6Al4V(ELI) samples (a) soaked at 20 $°C$ (b) soaked and tested till fracture at a temperature of 20 $°C$

The two figures show similar micrographs, both which exhibit globular α-grains, areas of lamellar, Widmanstätten, and bimodal microstructures. In Fig. 16(a), the average widths of the α-laths and β-laths were measured at 8.2±1.2 μm and 1.2±0.25 μm, respectively; while in Fig. 16(b) the average widths of the α-laths and β-laths were measured at 10.1±0.9 μm and 3.4±0.3 μm, respectively. The average widths of the α-laths and β-laths of the samples soaked at 20 $°C$ and then loaded in tension till fracture were observed to be wider than those of the sample that was only soaked at 20 $°C$. This is likely due to the heating effect due to loading and fracture of the specimens.

[DOI: 10.22068/ijmse.3589]

It was observed that as the soaking temperature and the testing temperature increased from 20 °*C* to 175 °*C*, the average widths of the α-laths and β-laths increased as well. This is consistent with the study by Shaikh *et al*. [18]. The recorded average widths of the α-laths and β-laths for the sample that was tested at a temperature of 175 °*C*, were 13.1±1.2 μm and 4.0±0.4 μm, respectively; while for the sample that was soaked at the temperature of 133 °*C* they were 8.3±1.4 μm and 1.8±0.45 μm, respectively. The higher average widths of the α-laths and β-laths for the former samples is noted. This is consistent with the studies by Zöllner [10], who reported that higher temperatures lead to coarsening of α-laths, while Shaikh *et al*. [18], observed an increase in the content of β-laths as the soaking temperature increased, as is observed in Fig. 15 and some parts of Fig. 16.

4. CONCLUSIONS

The aim of this study was to investigate the effect of temperature on the microstructure of the Ti6Al4V(ELI) alloy. The following conclusions were derived from the study.

- Stress relieve heat treatment does not change the original microstructure of acicular α' laths existing within columnar β-grain.
- High temperature annealing heat treatment significantly influences the microstructure of Ti6Al4V(ELI), as the α' laths are replaced by α- and β-laths.
- As the soaking temperature and the testing temperature are increased, the width of the α' lath, α-laths and β-laths increase as well.
- Increased tensile test temperature causes a decrease in the values of yield strength, ultimate tensile strength, modulus of elasticity, and hardness, as well as an increase in the values of ductility.
- For the samples that are tested in uniaxial tension, fracture comes with an increase of temperature, and an attendant increase in the widths of the α' laths, α-laths, and β-laths, which increase is greater near the fracture surface than at a distance of 15 *mm* away from the fracture surface.
- Fracture is accompanied by an increase in temperature and an attendant increase in the widths of the α' laths, α-laths, and β-laths compared to those of samples that are only soaked at different temperatures.
- Stress-relieved samples tested in tension at a temperature of 20 °*C*, had the highest yield and tensile strength, modulus of elasticity and hardness but lowest ductility. Samples that were stress relieved followed by high temperature annealing and then tested in tension at 350 °*C* had the highest ductility but lowest yield strength, ultimate tensile strength, modulus of elasticity, and hardness.

Clearly, changes in temperature does influence the microstructure and mechanical properties of Ti6Al4V(ELI). As the present work was a prelude to elevated temperature fatigue testing to determine whether these elevated test temperatures would affect the microstructures of the Ti6Al4V(ELI) samples, it can be said that changes in testing temperature are expected to influence the fatigue properties of the alloy. Moreover, the known heating effects arising from loading and failure of materials are expected to be exacerbated by fatigue loading.

ACKNOWLEDGEMENTS

This work is based on research supported by the South African Research Chairs Initiative of the Department of Science and Technology, the National Research Foundation of South Africa (Grant No. 97994), and the Collaborative Program in Additive Manufacturing (Contract No. CSIR-NLC-CPAM-21-MOA-CUT-03).

REFERENCES

[1] Wohlers Associates, *What is Additive Manufacturing*, Washington DC, 2010.

[2] Dehghanghadikolaei, A., Namdari, N., Mohammadian, B. and Fotovvati, B., "*Additive manufacturing methods, A brief overview*," *Journal of Scientific and Engineering Research*, 2018, 5, 123-131.

[DOI: 10.22068/ijmse.3589]

[3] Liu, S. and Shin, Y.C., "*Additive Manufacturing of Ti6Al4V alloy: A review*," *International Journal of Fatigue*, 2019, 164, 107552.
[4] Chadstand, V., Quagebeur, P., Maia, W. and Charkaluk, E., "*Comparative study of fatigue properties of Ti-6Al-4V specimens built by electron beam melting (EBM) and selective laser melting (SLM)*," *Materials Characterization*, 2018, 143, 76-81.
[5] Huang, H., Zhang, T., Chen, C., Hosseini, S.R.E., Zhang, J. and Zhou, K., "*Anisotropy in the Tensile Properties of a Selective Laser Melted Ti-5Al-5Mo-5V-1Cr-1Fe Alloy during Aging Treatment*", *Materials*, 2022, 15, 5493.
[6] Zhang, T., Huang, H., Hosseini, S.R.E., Chen, W., Li, F., Chen, C., Zhou, K., "*Obtaining heterogeneous α laths in selective laser melted Ti–5Al–5Mo–5V–1Cr–1Fe alloy with high strength and ductility*", *Materials Science and Engineering: A,* 2022, 835, 142624.
[7] Patterson, A.E., Messimer, S.L. and Farrington, P.A., "*Overhanging Features and the SLM/DMLS Residual Stresses Problem: Review and Future Research Need*," *Technologies*, 2017, 5, 15-38.
[8] Becker, T.H., Beck, M. and Scheffer, S., "*Microstructure and Mechanical Properties of Direct Metal Laser Sintered Ti6Al4V*," *South African Journal of Industrial Engineering*, 2015, 26, 1-10.
[9] Muiruri, A. M., "*Investigation of the High Strain Rate Behaviour and Impact Toughness of Ti6Al4V (ELI) Parts Built by the EOS M280 DMLS System with Standard Process Parameters; As-Built and Stress Relieved," MEng dissertation, Department of Mechanical and Mechatronics Engineering at Central University of Technology Free State, Bloemfontein*, 2018.
[10] Zöllner, D., "*Impact of a strong temperature gradient on growth in films*," *Modelling and Simulation in Material and Engineering*, 2022, 30, 16.
[11] Campbell, F., "*Fatigue and Fracture, Understanding the basics*", ASM International, Ohio, USA 2012, 415-447.
[12] Sterling, A., Shamsaei, N., Torries, B. and Thapson, S.M., "*Fatigue Behaviour of Additively Manufactured Ti-6Al-4V*," The 6th Fatigue Design Conference, Mississippi, 2015, 133, 576-589.
[13] Basuki, E.A., Prajitno, D.H. and Muhammad, F., "*Alloys Developed for High Temperature Applications*," Proceedings of the 1st International Process Metallurgy Conference (IPMC 2016), Bandung, 2017.
[14] Huo, Y., Yu, W., He, T., Hosseini, S.R.E., Ji, H., Bai, J., Chen, H. and Zhou, Z., *"Numerical Prediction and Experimental Investigation of Ductile Damage During Cold Upsetting of TC16 Titanium Alloy for Manufacturing Fasteners"*, *Transactions of the Indian Institute of Metals*, 2023, 76, 2963-2973.
[15] Zhao, J., Hung, F., Lui, T. and Wu, Y., "*The Relationship of Fracture Mechanism between High Temperature Tensile Mechanical Properties and Particle Erosion Resistance of Selective Laser Melting, Ti-6Al-4V Alloy*," *Metal*s, 2019, 9, 501-5015.
[16] Song, J., Han, Y., Fang, M., Hu, F., Ke, L., Li, Y., Lei, L. and Lu, W., "*Temperature sensitivity of mechanical properties and microstructure during moderate temperature deformation of selective laser melted Ti-6Al-4V alloy*," *Material Characterization*, 2020, 165, 110342.
[17] Sieniawski, J., Ziaja, W., Kubiak, K. and Motyka, M., "*Microstructure and Mechanical Properties of High Strength Two-Phase Titanium Alloys*," InTech, Poland, 2013.
[18] Shaikh, A., Kumar, S., Dawari, A., Kirwai, S., Patil, A. and Singh, R., "*Effect of Temperature and Cooling Rates on the α+β Morphology of Ti-6Al-4V Alloy*," The 2nd International Conference on Structural Integrity and Exhibition, Pune, 2018, 14, 782-789.
[19] Zherebtsov, S., Murzinova, M.A., Klimova, M.V., Salishchev, G.A., Popov, A.A. Semiatin, S.L., "*Microstructure evolution during warm working of Ti-5Al-5Mo-5V-1Cr-1Fe at 600 and 800°C*," *Material Science and Engineering*, 2013, 563, 168-176.
[20] Xu, J., Zhu, J., Fan, J., Zhou, Q., Peng, Y. and Guo, S., "*Microstructure and mechanical properties of Ti–6Al–4V alloy fabricated using electron beam freeform fabrication*," *Vacuum*, 2019, 167, 2019, 364-373.
[21] Ter Haar, G.M., Becker, T.H., Blaine, D.C., "*Influence of Heat Treatments on the Microstructure and Tensile Behaviour of Selective Laser Melting-Produced TI-6Al-4V*," *South African Journal of Industrial Engineering*, 2016, 27, 174-183.
[22] ASM International, "*Heat treating*," ASM International, Ohio, 2015.

[DOI: 10.22068/ijmse.3589]

[23] Reiners, W., Pyzalla, A.R., Schreyer, A. and Clemens, H., "*Microstructure and Properties of Engineering Materials*," *Neutrons and Synchrotron Radiation in Engineering Materials Science: From Fundamentals to Applications*, Wiley-VCH Verlag GmbH & Co. KGaA, 2017, 3-20.
[24] Pippan, R., Scheriau, S., Taylor, A., Hafok, M., Hohenwarter, A. and Bachmaier, A., "*Saturation of Fragmentation During Severe Plastic Deformation*," *Annual Review of Materials Research*, 2011, 40, 2322-2329.
[25] Lekoadi, P., Tlotleng, M., Maledi, N. and Masina, B.N., "*Improving the Microstructure of High Speed Selective Laser Melted Ti6Al4V Components by Varying residence time during Heat Treatment*," *University of the Witwatersrand, School of Chemical & Metallurgical Engineering*, Johannesburg, 2012.
[26] Madikizela, C., Cornish, L.A., Chown, L.H., and Moller, H., "*Microstructure and mechanical properties of selective laser melted Ti-3Al8V-6Cr-4Zr-4Mo compared to Ti-6Al-4V*," *Materials Science & Engineering*, 2019, 747, 225-231.
[27] Agius, D., Kourousis, K.I. and Wallbrink, C., "*A Review of the As-built SLM Ti-6Al-4V Mechanical Properties towards Achieving Fatigue Resistant Designs*," *Metal*, 2018, 8, 1-25.
[28] Phutela, C., Aboulkhair, N.T., Tuck, C.J. and Ashcroft, I., "*The Effects of Feature Sizes in Selectively Laser Melted Ti-6Al-4V Parts on the Validity of Optimised Process Parameters*," *Materials*, 2019, 13.
[29] Li, Y., Song, L., Xie, P., Cheng, M. and Xiao, H., "*Enhancing Hardness and Wear Performance of Laser Additive Manufactured Ti6Al4V Alloy Through Achieving Ultrafine Microstructure*," *Materials*, 2020, 13.
[30] Jazdzewska, M., Kwidzińska, D.B., Seyda, W., Fydrych, D. and Zieliński, A., "*Mechanical Properties and Residual Stress Measurement of Grade IV Titanium and Ti-6Al-4V and Ti-13Nb-13Zr Titanium Alloys after Laser Treatment*," *Materials*, 2021, 14.
[31] Malefane, L.B., "*Determination of the Fatigue Properties of Ti6Al4V(ELI) Parts Built By a Direct Metal Laser Sintering System with Standard Process Parameters Followed By Post-Processing Treatments*," Central University of Technology Free State, Bloemfontein, 2019.
[32] Jovanovic´, M.T., Tadić, S., Zec, S., Mišković, Z. and Bobić, I., "*The effect of annealing temperatures and cooling rates*," *Materials and Design*, 2006, 27, 192-199.
[33] Zhao, J., Wang, Z., Tian, L., Wan, J., Zong, X., Zhang, S., Zhao, H., Zhang, S. Zhao, H., "*Study on mechanical properties of Ti-6Al-4 V titanium alloy with different microstructures under combined tension-bending load*," *Journal of Alloys and Compounds*, 2022, 936.
[34] Zhang, H., Wang, C., Zhou, G., Zhang, S. Chen, L., "*Dependence of strength and ductility on secondary α phase in a novel metastable-β titanium alloy*," *Journal of Material Research and Technology*, 2022, 18, 5257-5266.
[35] Nalla, R., Ritchie, R.O., Boyce, B.L., Campbell, J.P. and Peters, J.O., "*Influence of Microstructure on high cycle fatigue of Ti6Al4V: Bimodal vs. Lamellar structures*," *Metallurgy and Material Transactions*, 2002, 33, 899–918.
[36] Benedetti, M. and Fontanari, V. "*The Role of Bimodal and Lamellar Microstructures of Ti-6Al-4V on the Behaviour of Fatigue Cracks Emanating from Edge-Notches*," *Department of Materials Engineering and Industrial Technologies*, University of Trento, Trento, 2004.
[37] Zha, M., Zhang, H., Yu, Z., Zhang, X., Meng, X., Wan, H. and Jiang, Q., "*Bimodal microstructure - A feasible strategy for high-strength and ductility materials*," *Journal of Materials Science & Technology*, 2018, 34, 257-264.
[38] Xing, L., Zhang, W., Zhao, C., Gao, W., Shen, Z. and Liu, W., "*Influence of Powder Bed Temperature on the Microstructure and Mechanical Properties of Ti6Al4V*," *Materials*, 2021, 14, 2278.

[DOI: 10.22068/ijmse.3589]